SOILPSI: a potential-driven three-dimensional soil water redistribution model—description and comparative evaluation

G.W. Theseira [a], G.E. Host [a,*], J.G. Isebrands [b], F.D. Whisler [c]

[a] *Natural Resources Research Institute, University of Minnesota Duluth, 5013 Miller Trunk Highway, Duluth, MN 55811, USA*
[b] *North Central Research Station, USDA Forest Service, 5985 Highway K, Rhinelander, WI 54501, USA*
[c] *Department of Plant and Soil Science, Mississippi State University, 117 Dorman Hall, Mississippi, MS 39762, USA*

Abstract

ECOPHYS, an individual-based process model for poplar, requires a three-dimensional soil water redistribution model to simulate soil water dynamics, plant uptake, and root growth. SOILPSI is a potential-driven water redistribution model based on the RHIZOS rhizosphere simulator. It expands on RHIZOS by calculating water flux based on water potential, and has a macropore flow mode to allow rapid drainage of the soil. SOILPSI simulates water flux in three dimensions and accounts for slope. SOILPSI was evaluated by comparing model output to soil moisture data collected under bare soil conditions. AMMI analysis of a date × depth matrix of differences between simulated and observed soil moisture content showed that excluding the two shallowest soil layers resulted in a difference matrix that conformed to an additive model. The grand mean predicted values were within 2% of the observed values, and 50 of 56 predicted values were within 5% of the observed values. Better agreements between simulated and observed soil moisture content were observed deeper in the soil profile and later in the season. Agreement between SOILPSI and field conditions was consistently more accurate than RHIZOS. Improving simulation of evaporative flux at the soil surface would improve simulation accuracy in the upper horizons.
© 2002 Elsevier Science Ltd. All rights reserved.

Software availability

Name of Software: SOILPSI

Contact address: G.E. Host, Natural Resources Research Institute, 5013 Miller Trunk Highway, Duluth, MN 55811, Tel.: +1-218-720-4264, fax: +1-218-720-4328, email: ghost@nrri.umn.edu

Year first available: 1998

Hardware required: IBM Pentium PC or equivalent with a minimum of 16 Mb RAM

Software required: MS Windows 95/98/2000/XP or NT

Program language: C/C++

Program size: 90K

Availability and cost: contact the developer for further information

1. Introduction

Forest crop process models, like agronomic models, require reliable submodels of belowground processes. Soil water redistribution is a critical process in simulating the movement of water and nutrients along the soil–plant–atmosphere-continuum. Accurate, multi-dimensional simulation of soil water redistribution is needed to facilitate implementation and testing of root growth, uptake and competition routines within mechanistic tree growth models. One such model is ECOPHYS, an individual tree, physiological process model for short rotation poplar that incorporates explicit calculation of light interception at the individual leaf level, response to varying CO_2, O_3 and temperature levels, dynamic carbon allocation, and varying crown architecture (Rauscher et al., 1990). We have developed a soil water redistribution model called SOILPSI to meet the belowground modeling needs of ECOPHYS to simulate root–shoot interactions within short rotation poplar plantations. Our linked

* Corresponding author. Tel.: +1-218-720-4264; fax: +1-218-720-4328.

E-mail address: ghost@nrri.umn.edu (G.E. Host).

model is based on a three-dimensional soil slab with a user-specified volume ranging from 1 to 50 m³. It is capable of simulating water addition to the soil slab via natural rainfall, irrigation or a water table, as well as water loss by evaporation or percolation through the bottom layer of the soil slab. SOILPSI was developed for a simulation cycle of approximately 10 years; the length of a short-rotation harvest cycle (Hansen, 1990, 1992). In this contribution, we describe SOILPSI and use it to simulate water dynamics in a soil of known physical and hydrologic properties, given the weather conditions from the 1991 growing season. We evaluate the model output in light of detailed soil moisture data collected from the actual soil during the same period (Theseira, 1994). We also provide a comparison of SOILPSI and RHIZOS, a widely used agronomic crop model (Boone et al., 1995) that served as the basis for SOILPSI.

2. Modeling approach

2.1. Introduction and general model description

The variety of modeling approaches and methods used by scientists is a result of the complexity of biological systems, differences in modeling priorities, methodological trade-offs, strategies for bridging information gaps and, sometimes, academic tradition (Sharpe, 1990). The RHIZOS soil model has been well documented (Boone et al., 1995) and has been selectively utilized in several agronomic crop models such as GOSSYM (Baker et al., 1983), GLYCIM (Acock and Trent, 1991), and CALGOS (Marani et al., 1992). We selected RHIZOS as a template for construction of our new model for several reasons. The CERES-type crop models of Jones and Kiniry (1986), the SWIF forest models (Bouten and Witter, 1992), the BEANGRO, SOYGRO, and PNUT-GRO group of models (Hoogenboom et al., 1992) all utilize one-dimensional soil processes. RHIZOS, on the other hand, simulates soil processes in two-dimensions that correspond to a one-unit thick cross-section of the crop row. We did not consider crop models that simulate soil water as available and/or unavailable pools without regard to spatial differentiation. Other crop models of the EPIC/ALMANAC (Williams et al., 1983) group or the QB-Maize models (Sinclair, 1991) simulate the plant as a collection of biomass pools with no spatial component. RHIZOS, however, possesses a belowground framework that permits precise location of discrete root segments from one or more distinct plants. Stand level forest models such as PROGNOSIS (Schuster et al., 1993) were not considered because they lacked the ability to model individual trees.

SOILPSI and the RHIZOS (Boone et al., 1995) soil model on which it is based share the detailed spatially explicit modeling approach of the ECOPHYS model

(Rauscher et al., 1990). Our approach espouses the development of fine-scale, mechanistic models of individual soil–root–tree–air systems, which are consequently scaled to patches, and thereafter, plantations of poplar trees (Host et al., 1996). In this approach, stochastic behavior is generated through inter-tree competition for resources in the soil slab. This scenario is similar to the 'aggregation' technique suggested by Acock and Reynolds (1990) in which a heterogeneous ecosystem is simulated using single tree models. In our approach, however, a single soil slab may support a patch of trees in direct competition. We can then simulate a plantation by using multiple patches of variable composition (Host et al., 1996).

It is generally accepted that the detail and accuracy of any model is constrained by that of its component modules. Because the ECOPHYS tree is discretely programmed in three-dimensional space, we chose to develop a model with a three-dimensional soil slab (Host et al., 1996). This architecture was designed to accommodate our three-dimensional discrete root segment model currently functioning in ECOPHYS. With these goals in mind, SOILPSI was developed, as a scaleable, three-dimensional soil slab comprising a collection of individual soil cells or voxels. The absolute size of individual voxels is user-defined (e.g. 1–5 cm³) to allow trade-offs between model resolution and computational intensity. Water potential equilibration may be simulated in one, two or three directions and can account for soil slope. The model employs an hourly time step for water content equilibration, drainage and water uptake by plant roots. This time step synchronizes SOILPSI with plant functions in ECOPHYS such as light interception, photosynthesis, stomatal conductance, and consequently, anticipated transpiration demand. Hourly or daily time steps may be used for infiltration and evaporation, depending on the resolution of rainfall, solar radiation and temperature data available in the simulation.

2.2. Macropore flow

The role of macropores in infiltration and drainage is receiving increased attention. This is evidenced by the work of Glass et al. (1989), Hillel and Baker (1988), and Beven and Germann (1982), and more recent studies by Heijs et al. (1995), Li and Ghodrati (1995), and Ghodrati and Jury (1992). To date, however, all characterization attempts have required physical examination of the structure and distribution of macropores of the soil in question, and no method has been developed to estimate soil water behavior in macropores from readily available soil physical properties such as a desorption curve. While it is generally understood that water flow in soils wetted above field capacity occurs in both macropores and micropores, SOILPSI treats infiltration and drainage as macropore functions. SOILPSI incorporates the piston

flow infiltration mechanism used in RHIZOS (Boone et al., 1995), but adds an algorithm to iteratively distribute infiltrating water equally to all non-saturated soil voxels (in two dimensions) at the wetting front during any infiltration event. Voxels of the deepest infiltrated layer in RHIZOS are sequentially saturated in one dimension beginning under the furrow. Saturation progresses toward the crop row until all infiltrating water is allocated.

SOILPSI simulates drainage of soil water at a potential of greater than −0.03 MPa as macropore flow. Drainage or percolation occurs between a soil voxel and the one immediately below it, and is regulated by the amount of void pores in the sink voxel. If the water table is below the soil slab, drained water is permitted to exit the slab. If the water table occurs within the soil slab, it is treated as a sink for drained water. In either case, the water table functions as an infinite sink for drainage and as an infinite source of water when soil water potential in the overlying soil falls below −0.03 MPa.

2.3. Micropore flow

All soil water in SOILPSI is subject to three-dimensional, potential gradient based equilibration. During each time step, micropore flow based on soil water potential difference is superimposed on any macropore flow that might have occurred during that time step. We calculate the matric potential of two adjacent soil voxels (Fig. 1) from their volumetric water content with the soil water content–soil water potential relationship given by (1), developed by van Genuchten (1980):
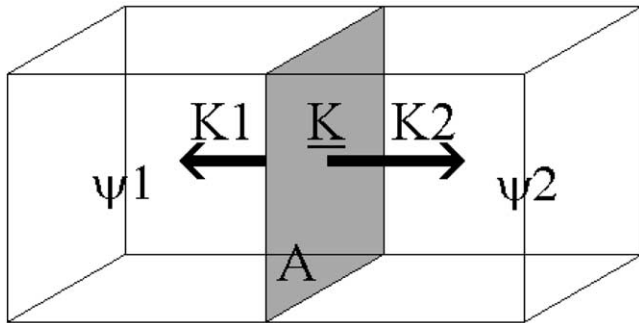
K1 - hydraulic conductivity of left cell
K2 - hydraulic conductivity of right cell
$\underline{K}$ - geometric mean hydraulic conductivity
A - surface area across which flow occurs
Ψ1 - hydraulic head (potential) of left cell
Ψ2 - hydraulic head (potential) of right cell

Fig. 1. Flux between adjacent soil voxels is calculated using the potential difference between the voxels and the geometric mean conductivity of the voxels.

$$\theta_i = \frac{\theta_r + (\theta_s - \theta_r)}{(1 + (|a_i|)^b)^g},\tag{1}$$

where θ_i is the volumetric water content, Ψ_i the pressure head (cm), θ_r the residual volumetric water content, θ_s the saturated volumetric water content, a the coefficient which has units of reciprocal pressure head (length^{-1}), b a dimensionless coefficient, and g is a dimensionless coefficient related to b by $g = 1 - (1/b)$. If any difference in elevation exists between the voxels, e.g. if the voxels were one above the other, or side by side in the direction of the soil slope, a commensurate gravitational potential is added to the potential difference between the voxels. The hydraulic conductivity used in calculating the flux between the soil voxels is calculated using Eq. (2) (van Genuchten, 1980):

$$K = K_{sat}(s)^{0.5}(1 - (1 - s^{ovm})^g)^2,\tag{2}$$

where K is the hydraulic conductivity (cm h^{-1}), K_{sat} the saturated hydraulic conductivity (cm h^{-1}), $s = (\theta - \theta_r)/(\theta_s - \theta_r)$, g as defined in Eq. (1) previously, and ovm $= 1/g$.

The unsaturated hydraulic conductivities of source and sink voxels can vary by many orders of magnitude. Because the arithmetic mean weights larger conductivity values over smaller ones, we use the geometric mean conductivity to calculate the inter-voxel flux. On the other hand, the estimation of hydraulic conductivity using the geometric mean can raise problems when an extremely dry sink voxel radically attenuates the geometric mean conductivity. Where the source and sink voxels are equally dry, low conductivity is acceptable, but where the source voxel is between saturation and field capacity, the outcome of the geometric mean calculation does not reflect the true conductivity between the voxels. When this occurs, we assume that a wetting front exists between the voxels and that the flux is regulated more by the high potential condition immediately behind the wetting front than the low potential condition ahead of it. Consequently, the conductivity of the source voxel is used to calculate the resultant flux between the source and sink voxels. If the magnitude of the flux between the two voxels is such that a water potential equilibrium will be achieved during that time step (hour), voxel water content values are back calculated from the equilibrium potential, and the sum of the water in the voxels is proportionately allocated. Otherwise, the calculated flux is applied and water is redistributed.

2.4. Water uptake by tree roots

We simulate a root system as a binary tree assemblage of root segments whose ends (nodes) are defined by coordinates in three-dimensional Cartesian space. This modeling approach is similar to that of Diggle (1988). The coordinates of the distal node of each root segment

define the soil voxel in which it is located (Fig. 2). In addition, each root segment has an age property that is used to determine the root's persistence, given its anticipated longevity. We simulated uptake in a method similar to that used for soil water redistribution. Root diameter is modeled as a function of age, and growth photosynthate is allocated according to the pipe model theory (constant total cross-sectional area for transport) proposed by Shinozaki et al. (1964). The length and diameter of the root segment determine the surface area through which transport may occur, while the age cohort of the root determines the radial conductivity per unit surface area of root. We establish a potential gradient between the soil voxel and the plant root, and calculate a soil to root water flux for a given soil voxel for that time step. Because the model can distinguish between the roots of individual trees, the proportions of nodes from different trees, coupled with individual tree water potentials, determines their competitive ability in a given soil voxel. At the present time, transpiration demand imposes a uniform matric potential on the entire root system and potential differences within the root system occur as a consequence of elevation of individual root segments only (all roots within a given soil voxel possess the elevation of that soil voxel).

2.5. Evaporation from the soil surface

We patterned the evaporation subroutine after the modified Penman model used in RHIZOS. We first calculate potential evaporation using the Penman Equation. We then calculate actual evaporation based on the soils' ability to supply water to meet evaporative demand (Boone et al., 1995). A critical input variable is the air–dry soil moisture content, which is the level of soil moisture at which no more water will be relinquished to the atmosphere. Air–dry soil moisture content of surface horizons can be estimated through simple drying experi-
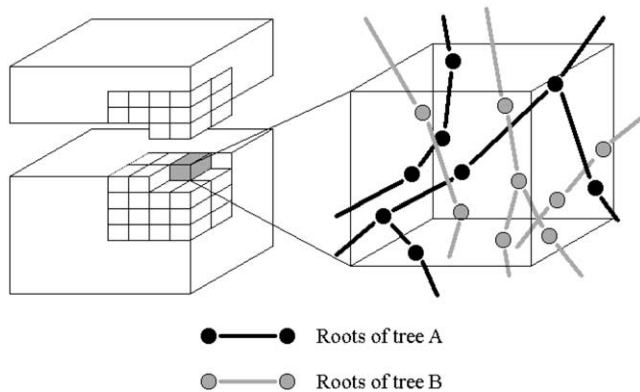

Fig. 2. Cutaway of the soil slab depicting colonization of a given soil voxel by roots from separate trees. Relative node density determines competitiveness of a given tree for the water contained in the soil voxel.

ments. In the event that such data are unavailable, the user may specify a matric potential to which water may be extracted.

2.6. Model inputs and outputs

The primary inputs to the model consist of hourly weather data, soil properties, and several model control parameters (Table 1). The simulation control parameters specify the duration of the simulation, the number of dimensions and the spatial resolution at which water movement in the slab will be simulated. Hourly weather data can be read directly from a file or generated using a weather generator such as WGEN (Richardson and Wright, 1984). Model output consists of a one-, two- or three-dimensional array of soil moisture values, depending on user selection.

An example of a 96-h simulation of a soil slab is depicted in Fig. 3. In this simulation, the slab is initiated at a uniform soil water content (field capacity) corresponding to green in the color plates. To simulate evaporation, strong negative water potential is specified at the

Table 1
List of SOILPSI simulation inputs

| Input	Data range	Units
Length of simulation	>1	h
Number of dimensions in which to equilibrate	1–3	Dimensions
Slab dimensions		
Length	>1	m
Width	>1	m
Depth	>1	m
Slab slope		
Primary	0–45	Degrees
Secondary	0–45	Degrees
Number of horizons	>0	Horizons
Depth to water table	0-Slab depth	m
Initial soil slab water content		
One-dimensional	0-Saturation	$m^3 \, m^{-3}$
Two-dimensional	0-Saturation	$m^3 \, m^{-3}$
Three-dimensional	0-Saturation	$m^3 \, m^{-3}$
Individual horizon properties		
Thickness	>0	cm
Saturated volumetric water content	0–1	$m^3 \, m^{-3}$
Residual volumetric water content	0–1	$m^3 \, m^{-3}$
Saturated hydraulic conductivity	>0.0	$cm \, h^{-1}$
Horizon α	Generated	cm^{-1}
Horizon β	Generated	Dimensionless
Horizon λ	Generated	Dimensionless
Hourly solar radiation	0–2000	$\mu mol \, m^{-2} \, s^{-1}$
Hourly rainfall	≥0	$mm \, h^{-1}$
Hourly irrigation		
Non-point source	≥0	$mm \, h^{-1}$
Point source (source coordinates)	≥0	$mm \, h^{-1}$
Sink cells		
Point sink (sink coordinates)	<0	$cm \, H_2O$ (tension)
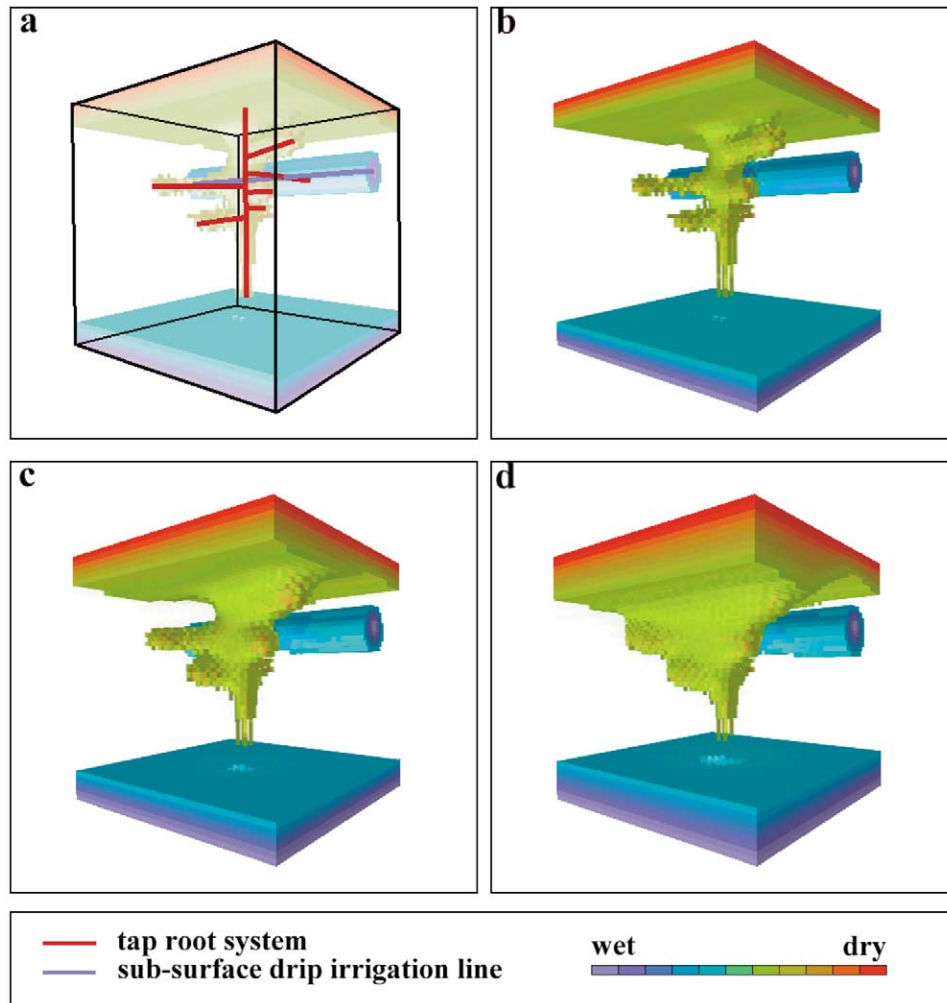
Fig. 3. Graphical representation of data output of a 96-h simulation of a soil slab (a) containing a tap root system and subsurface drip irrigation line. Boundary conditions include surface drying by evaporation, a water table at the base of the slab, constant irrigation rate and constant water potential in the root system. The slab was initialized with a uniform median water content (green), which was rendered transparent in (b)–(d). In this simulation the drying front advances downward from the soil surface and outward from the root system, while the wetting front advances upward from the water table and outward from the irrigation line at (b) 24, (c) 48 and (d) 96 h.

upper surface of the soil slab. A water table, at zero water potential, is specified as the lower boundary of the soil slab. In addition, an array of voxels with negative water potential was inserted to simulate a plant root system, while another zone of voxels experiences an addition of a fixed volume of water each time step to simulate a subsurface drip irrigation line (Fig. 3(a)). When the color green is rendered transparent in Fig. 3(b), (c) and (d), the range of colors from yellow to red depict the advance of a drying front downward from the soil surface, and outward from the root system at 24, 48, and 96 h, respectively. During the same interval, the blue color range depicts the progression of a wetting front upward from the water table (consistent with capillary rise) and outward from the subsurface drip irrigation line.

2.7. Other modeling considerations

We coded SOILPSI in C++ to take advantage of object oriented programming techniques and to interface with the COM-based, object oriented C++ code of ECO-PHYS (Host et al., 1999; Isebrands et al., 2000). We define the soil slab as an object class with member methods that permit the slab to infiltrate, drain, and equilibrate. In this way, we can create many instances of a soil slab to simulate a plantation with heterogeneous soils (Host et al., 1999).

At the present time, we have not implemented changes in soil physical characteristics due to freezing and thawing cycles. Soil water redistribution is deactivated when the soil temperature is below freezing.

3. Model evaluation

3.1. Field methods

There is a general paucity of published data on three-dimensional water movement and distribution in a natural soil profile throughout a growing season. This is primarily because of the large labor and equipment requirement necessary to install, maintain and monitor a large three-dimensional grid of soil moisture sensors through a growing season. Data at scales covering one or more square meters in area and extending a meter or more into the soil are particularly scarce. A recent study of multi-dimensional water flow utilized excavated and repacked soils as well as in situ measurements beneath a crop row (van Genuchten et al., 1991). While a dense grid of sensors was employed, the use of reconstructed soils added the possibility of altered physical and hydrologic properties. In addition, the volume of soil monitored has been relatively small (0.7 m deep and extending 0.4 m laterally from the crop row). Furthermore, because the study focused on water uptake by plant roots, water redistribution due solely to soil factors was confounded by root extraction of soil water.

The field data we used for testing SOILPSI is part of a larger data set collected to compare two-dimensional water profiles under bare soil or cotton (*Gossypium hirsutum*) cropped conditions, and three irrigation regimes (Theseira, 1994). The study was conducted at the Mississippi Agriculture and Forestry Experiment Station research plots located on the north farm at Mississippi State University during the 1991 growing season. The soil was Marietta silt-loam (fine, loamy, siliceous, thermic, Fluvaquentic, Eutrochrept) with less than 2% slope with three horizons. The boundary between the A and B1 horizons occurred at a mean depth of 0.15 m and the B1–B2 horizon boundary occurred at 0.4 m. The plot design was a randomized complete block containing six blocks and three irrigation regimes (no irrigation, standard furrow irrigation, and alternate furrow irrigation). However, no irrigation was applied due to excessive rain, such that each block contained three replicate samples.

Families of 0.6, 0.9, and 1.22 m long piezometer tubes indicated a seasonal mean water table depth of 1.1 m. We installed neutron probe access tubes in each of the 18 plots as described in Fig. 4(a)–(c). These were read on weeks 5, 6, 7, 10, 12, 14, 15 and 16 of the study for a total of eight sampling dates. Each tube was read at 25, 40, 55, 70, 85, and 100 cm below the soil surface. In addition, we collected a surface soil moisture sample in each plot using a soil sampler of known volume, resulting in soil water content measurements at seven depths for each sampling interval (Fig. 5.) This provided us with soil water content measurements at seven soil depths.
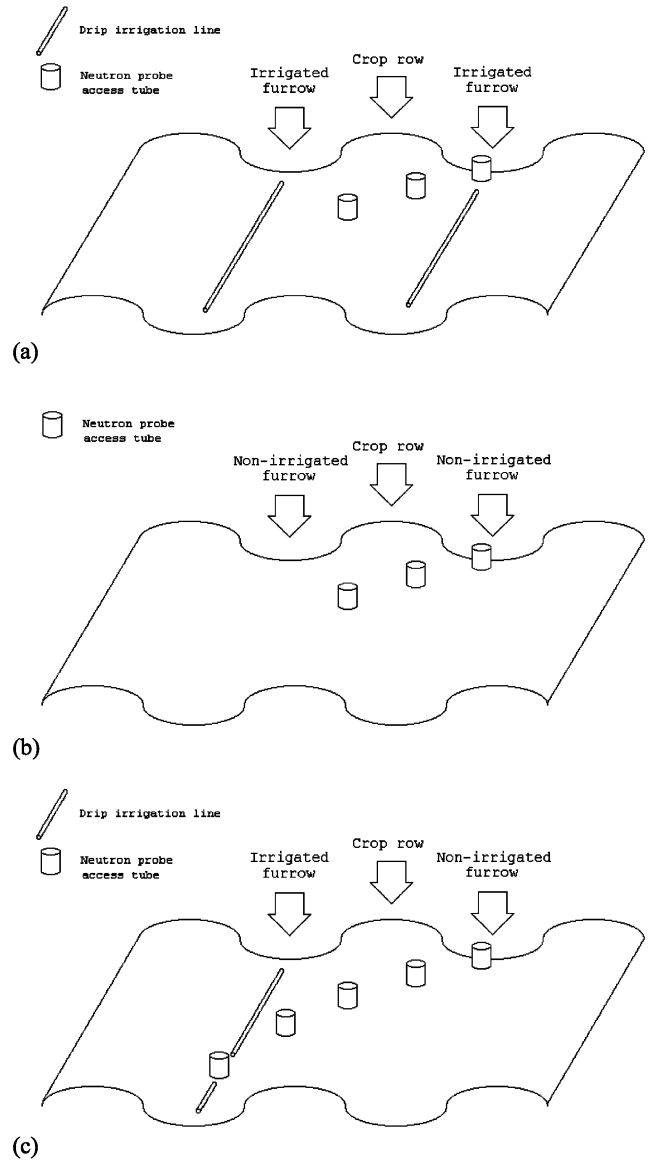

Fig. 4. Location of neutron-probe access-tubes and drip irrigation lines in (a) standard drip irrigated, (b) non-irrigated and (c) alternate furrow irrigated plots.
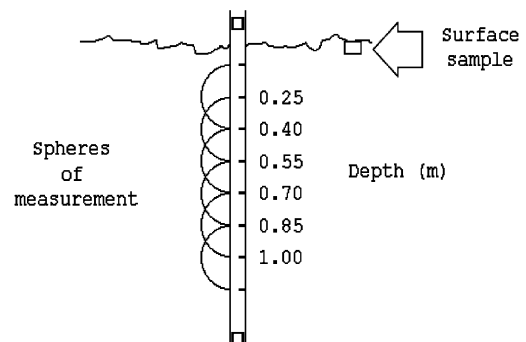

Fig. 5. Depths at which soil moisture was measured with the neutron moisture meter and fixed volume surface soil sampler.

3.2. RHIZOS and SOILPSI simulations

We conducted pressure plate desorption analyses on soil samples taken from the study site to obtain paired soil water content and matric potential values. We then used the RETC program (van Genuchten et al., 1991) to generate the constants that characterize the soil water content/soil water potential relationship as well as hydraulic conductivity. These constants were used to parameterize the simulated soils for both the RHIZOS and SOILPSI models.

We simulated hourly soil water dynamics within a 2-m deep soil slab underlying a bare soil surface with RHIZOS and SOILPSI using 1991 weather traces recorded at the Mississippi Agriculture and Forestry Experiment Station at Mississippi State, Mississippi. Because RHIZOS is not capable of stand-alone simulation, the model was run within the 1991 release of the GOSSYM cotton model without a cotton crop (Boone et al., 1995). In both RHIZOS and SOILPSI simulations, a water table was specified at 1.1 m in accordance with piezometer observations. We also specified a constant water potential limit of 1.5 MPa for evaporation loss from the soil surface, based on laboratory measurements of field samples.

3.3. Statistical methods

Model prediction accuracy was evaluated using the Additive Main Effects-Multiplicative Interaction (AMMI) procedure. AMMI analysis has been frequently applied to experimental designs where true replication of experimental units is implausible. AMMI analyses have been used independently (Abamu et al., 1998; Abamu and Alluri, 1998; Yadav et al., 1998; Annicchiarico, 1997a; Oritz, 1996) or in combination with other more traditional statistical methods (Annicchiarico, 1997b; Flores et al., 1996; Falkenhagen et al., 1996). Willers et al. (1995), applied AMMI analyses to two-way soil moisture data (depth by row position) to evaluate the difference between measured and predicted soil moisture at each depth/row position combination. In doing so, they demonstrated that AMMI analyses could be used to test differences between deterministic computer model output and field observations if the data conformed to a two-way treatment structure. We used the AMMI analysis to identify depths and date interactions and to evaluate a 7×8 (soil depth by sampling date) matrix of differences between observed water content values (plot means) and model predictions (Table 2).

4. Results and discussion

4.1. Simulations evaluated

We found that approximately 14% of the elements in the difference matrix had a 5% confidence interval that included zero, indicating that simulation output did not differ significantly from field data. These elements were grouped at the deeper depths in the soil, and later in the growing season. The remaining elements, as well as the row and column means and the grand mean had confidence intervals that did not include zero, indicating that simulation output differed significantly from field data. The 5% confidence interval described subsequently, however, was rather strict, generally requiring differences between predicted and observed values to be less than 1%.

The characteristic root test for interaction (Milliken and Johnson, 1989) was used to test for interaction in the 7×8 data matrix. The hypotheses Ho: $\lambda_1 = 0$, and Ho: $\lambda_2 = 0$, where λ_1 and λ_2 are the coefficients of the first and second multiplicative terms, respectively, were rejected at the 0.01 critical point, indicating the presence of interacting rows and/or columns. To gauge the pattern of interaction, we generated type I and II interaction plots of the data (Milliken and Johnson, 1989) using depth and sampling date as the baseline. We also plotted the AMMI residuals (difference between the data and the predictions of the additive model) using the two baselines described previously. The type I and II interaction plots showed strong interaction between the first and second depths and the rest of the depths. The residuals plot showed that the magnitude and direction of the residuals varied when either depth or date of sampling was used as the baseline. In particular, the high degree of variability in the residuals at the shallowest depth, and to a lesser degree, the second depth, indicates that the model responds differently at those depths than it does for the other data points in the matrix.

Further characteristics of the interactions are shown in the first and second set of eigenvectors associated with the date and depth of sampling (Tables 3 and 4, respectively). The eigenvectors associated with date of sampling (Table 3) indicates that the second and possibly, the fourth sampling dates differ in response compared with the other sampling dates. The second set of eigenvectors point particularly to the difference in response between the fourth and fifth sampling dates. The two sets of eigenvectors associated with depth (Table 4) corroborate the residual analysis described previously: the first and second sets of eigenvectors reflect differences in the response of the shallowest and second soil layers, respectively.

Removing the first and second depths from the difference table (Willers et al., 1995) and rerunning the characteristic root test for interaction revealed that significant interaction was absent from the remaining difference table. We then used the variance of the refitted model to construct $1-\alpha(\alpha = 0.05)$ confidence intervals for individual matrix elements, column means, row means and the grand mean to test equivalency to zero (Table 5). The 5% confidence intervals were rather strict,

Table 2
Differences between observed and simulated volumetric soil moisture content (%)

Date of sampling	Depth of sampling						
	1	2	3	4	5	6	7
1	−8.25	2.69	−2.96	−1.70	−1.14	−1.23	−0.85
2	−11.69	2.75	−2.48	−0.89	−0.74	−0.71	−0.49
3	−4.99	4.19	−2.44	−1.54	−1.48	−1.48	−0.86
4	−7.83	4.46	−3.15	−1.92	−2.15	−2.12	−1.15
5	−4.93	2.18	−2.95	−1.70	−2.02	−2.13	−0.43
6	−9.77	2.47	−3.11	−1.72	−1.76	−1.75	−0.32
7	−8.14	2.41	−2.66	−1.78	−1.89	−2.31	−1.41
8	−7.84	2.54	−3.59	−2.39	−3.16	−3.41	−1.97

Table 3
First and second eigenvectors associated with date of sample collection

	Eigenvector set	
	First	Second
1	0.1055	−0.1968
2	0.7017	−0.0617
3	−0.3996	0.2039
4	−0.0579	0.7009
5	−0.4580	−0.5880
6	0.2964	−0.1475
7	0.0012	−0.1184
8	−0.1894	0.2076

Table 4
First and second eigenvectors associated with depth of sample

	Eigenvector set	
	First	Second
1	0.9019	−0.1697
2	0.0132	0.9101
3	−0.0992	−0.0442
4	−0.1717	−0.0870
5	−0.2432	−0.1866
6	−0.2619	−0.1430
7	−0.1390	−0.2795

Table 5
Confidence intervals for grand mean, row mean (sampling depth), column mean (sampling date) and individual element means

	Confidence interval (%)
Grand mean	±1.10
Row mean (mean of seven depths)	±0.42
Column mean (mean of eight sampling dates)	±0.39
Individual cells (single depth/sampling date combination	±1.10

date. None of the row or column means had confidence intervals that include zero. In the same way, the confidence interval of the grand mean did not include zero. This evaluation shows that SOILPSI leaves the soil surface too wet (high negative differences in depth 1), while depth 2 is too dry (positive differences). These layers are the primary source of interaction in the difference table. The remainder of the table (depths 3–7) shows a more uniform negative difference, indicating that SOILPSI water content predictions are generally higher than observed values by between 1 and 3% in a majority of the date-by-depth of sampling combinations. These relatively small differences provide confidence that the SOILPSI model performs well under non-cropped conditions. In contrast, only 22 of the 56 values (59%) from the RHIZOS simulation fell within 5% of the observed values. Only two of the 56 matrix elements met the limits of the 5% AMMI confidence interval. Moreover, RHIZOS recorded a grand mean error in excess of 14%, compared to a −2.03% grand mean error for SOILPSI.

4.2. Experimental considerations

Examination of the change in moisture content in the field compared with SOILPSI and RHIZOS predictions following rainfall events yields valuable information about model performance during wetting and drying

ranging from 0.39% for the sampling dates means to 1.1% for the grand mean.

Table 6 shows the percent difference between SOILPSI prediction vs. field observations by date and depth. Fifty of 56 values (89%) fell within 5% of the observed value, and most of the predictions were within 2–3% of observed values. Eight of 56 matrix elements (14%) fit the strict limits (0.39–1.10%) imposed by a 5% AMMI confidence interval. These elements were concentrated primarily in depth 7 or in the second sampling

Table 6
Differences between observed and simulated volumetric soil moisture content (%) showing individual element values and row, column and grand means

Date of sampling	Depth of sampling							
	1	2	3	4	5	6	7	Mean
1	−8.25	2.69	−2.96	−1.70	−1.14	−1.23	−0.85∗	−1.92
2	−11.69	2.75	−2.48	−0.89∗	−0.74∗	−0.71∗	−0.49∗	−2.04
3	−4.99	4.19	−2.44	−1.54	−1.48	−1.48	−0.86∗	−1.23
4	−7.83	4.46	−3.15	−1.92	−2.15	−2.12	−1.15	−1.98
5	−4.93	2.18	−2.95	−1.70	−2.02	−2.13	−0.43∗	−1.71
6	−9.77	2.47	−3.11	−1.72	−1.76	−1.75	−0.32∗	−1.44
7	−8.14	2.41	−2.66	−1.78	−1.89	−2.31	−1.41	−2.25
8	−7.84	2.54	−3.59	−2.39	−3.16	−3.41	−1.97	−2.83
Mean	−7.93	2.96	−2.92	−1.71	−1.79	−1.89	−0.93	−2.03

∗Indicates that the $\alpha = 0.05$ confidence interval about the mean includes zero

cycles. The differences between the times of peak water content at a given soil depth show if the model is running ahead of, or lagging behind, field conditions. Furthermore, times at which the model begins to deviate from field conditions can point to weaknesses in the model and oftentimes reveal how it needs amendment. It is important to note that while RHIZOS and SOILPSI generated daily and hourly data, respectively, field conditions permitted soil moisture sampling only on discrete dates. Temporal patterns of soil moisture content from the field and model simulations at seven depths are presented in Fig. 6. Significant rain events during the growing season are also depicted.

With the exception of the soil surface, soil moisture content under bare soil conditions ranged between 0.25 and 0.43 $m^3 m^{-3}$ near saturation (during rainfall, and not evident due to the interpolation curve). For this soil type, water potential near field capacity was −0.033 MPa. When the RHIZOS model deviated from field values, it erred to the wet side of the soil moisture spectrum, gradually increasing in error until water contents reached values close to saturation (Fig. 6). In essence, RHIZOS has difficulty draining water from voxels that are at or above field capacity at the rate that soil is drained in the field. In contrast, the SOILPSI simulations significantly overestimated the soil moisture content at the soil surface, slightly overestimated soil moisture at the 0.4, 0.55, 0.7, 0.85 and 1.0 m depths, and marginally underestimated water content at the 0.25 m depth (Fig. 6). The overestimation of moisture content at the soil surface was due to the specified minimum dry-down value for the surface horizon. Empirical determination of air–dry soil moisture values would improve the prediction of moisture content at the soil surface. Note also that the 0.25-m depth (depth 2) supplied water to the surface to meet evaporative demand (days 198 and 218) once the surface drying limit was reached. A more accurate deter-
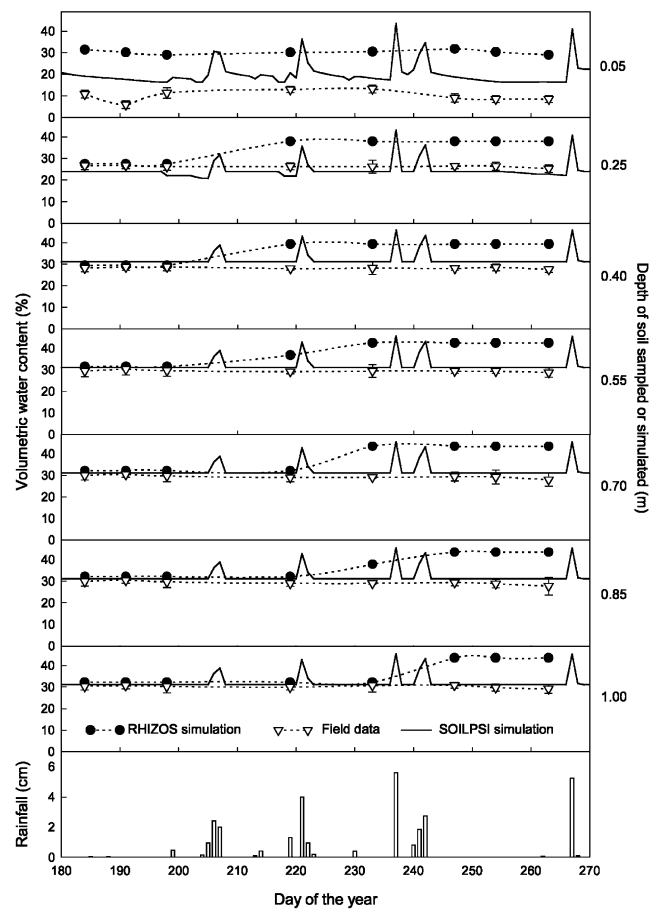

Fig. 6. Observed (pooled row position means) and simulated (RHIZOS and SOILPSI) soil moisture content at seven depths beneath a bare soil surface. Observed data and RHIZOS output are on eight selected days while SOILPSI output are daily maxima generated from hourly data. Error bars on observed data denote one standard deviation.

mination of surface air–dry moisture content would thus improve model predictions at subsurface horizons as well.

The drainage and wetting front algorithms of SOILPSI, combined with potential-driven soil water redistribution appear to solve the problem of water retention at levels exceeding field capacity observed in RHIZOS. To illustrate this, a 12-h simulation of a water pulse applied to soil at field capacity is shown in Fig. 7. The pulse moves through the upper 1 m of soil in approximately 10 h. The surface soil moisture content was below field capacity prior to the rain, and was wetted to field capacity by the event. This wetting resulted in a decrease in the amplitude of the water pulse in the deeper depths. The remainder of the soil, however, was already at field capacity. As a consequence, no change in moisture content was noted as the pulse moved through each layer. Field evaluation of this phenomenon would require hourly measurements of soil water following rainfall to characterize the depth-specific rates of decay of water content to a quasi-equilibrium state.

5. Conclusion

The SOILPSI model uses water potential to redistribute water within a three-dimensional soil matrix on an hourly time step. It accounts for both macropore and micropore flow, and resolves a long-standing problem in simulating water movement at the wetting front. In a comparison of model predictions and field data, the predictions were generally within 2–3% of the observed values. The largest prediction errors occurred in the surface horizon, where a lack of a good estimate of air–dry soil moisture led to an overestimation of soil moisture content. Future activities in model development will focus on root extraction of soil water as driven by transpiration demand from the ECOPHYS canopy and expressed through the root distribution throughout the soil slab.
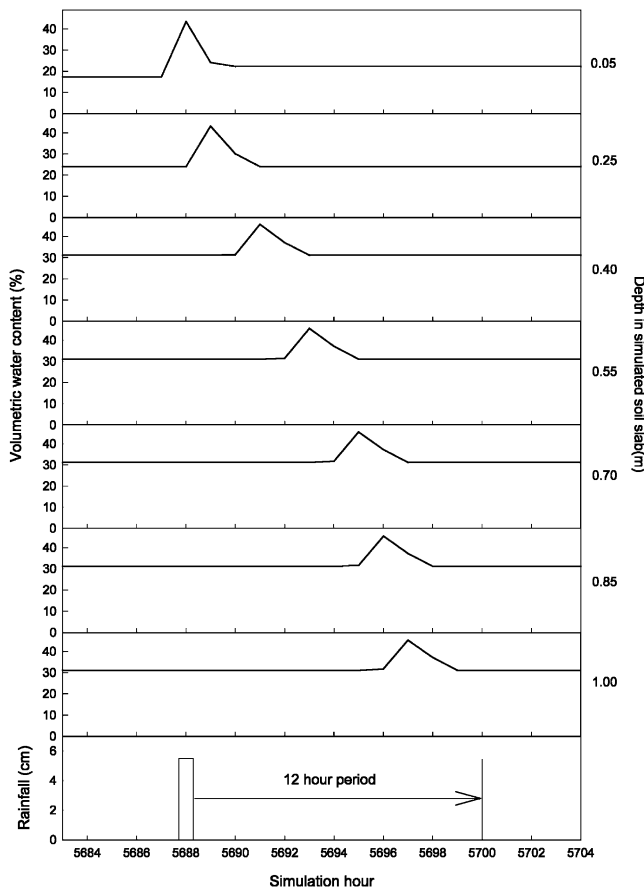
Fig. 7. SOILPSI simulation depicting a pulse of elevated soil water content at seven soil depths during the hours following a rain event. Note the increase in surface soil moisture content following the event. Subsurface layers were at field capacity and therefore show no increase in wetness following passage of the water pulse.

References

Abamu, F.J., Akinsola, E.A., Alluri, K., 1998. Applying AMMI models to understand genotype-by-environment (G × E) interactions in rice reaction to blast disease in Africa. International Journal of Pest Management 44 (4), 239–245.

Abamu, F.J., Alluri, K., 1998. AMMI analysis of rainfed lowland rice (*Oryza sativa*) trials in Nigeria. Plant Breeding 117 (4), 395.

Acock, B., Reynolds, J.F., 1990. Model structure and data base development. In: Dixon, R.K., Meldahl, R.S., Ruark, G.A., Warren, W.G. (Eds.), Process Modeling of Forest Growth Responses to Environmental Stress. Timber Press Inc., Portland, OR, USA, pp. 169–179.

Acock, B., Trent, A., 1991. In: The Soybean Crop Simulator, GLYCIM: Documentation for the Modular Version 91. Department of Plant, Soil and Entomological Sciences, University of Idaho, Idaho, Moscow, 242.

Annicchiarico, P., 1997a. Additive main effects and multiplicative interaction (AMMI) analysis of genotype-location interaction in variety trials repeated over the years. Theoretical and Applied Genetics 94 (8), 1072.

Annicchiarico, P., 1997b. Joint regression vs. AMMI analysis of genotype-environment interactions for cereals in Italy. Euphytice; Netherlands Journal of Plant Breeding 94 (1), 53–62.

Baker, D.N., Lambert, J.R., McKinion, J.M., 1983. GOSSYM: a simulator of crop growth and yield. In: Technical Bulletin 1089. South Carolina Experiment Station, Clemson University, Clemson, South Carolina, USA, 134.

Beven, K., Germann, P., 1982. Macropores and water flow in soils. Water Resources Research 18, 1311–1325.

Boone, M.Y.L., Porter, D.O., McKinion, J.M., 1991. In: RHIZOS 1991: A Simulator of Row Crop Rhizospheres. US Department of Agriculture, Agricultural Research Service, ARS-113, USA, 180.

Bouten, W., Witter, J.V., 1992. Modeling soil water dynamics in a forested ecosystem II: evaluation of spatial variation of soil profiles. Hydrological Processes 6, 435–444.

Diggle, A.J., 1988. Rootmap: a root growth model. Mathematics and Computers in Simulation 30, 175–180.

Falkenhagen, E., Funnah, S.M., Du Toit, W., 1996. A comparison between the linear regression and AMMI approaches to study multi-site trials using a sample of South African maize trials. South African Journal of Plant and Soil 13 (4), 103–109.

Flores, F., Moreno, M.T., Martinez, A., Cubero, J.I., 1996. Genotype-environment interaction in faba bean: comparison of AMMI and principal coordinate models. Field Crops Research 47 (2-3), 117–127.

Ghodrati, M., Jury, W.A., 1992. A field study of the effects of soil structure and irrigation method on preferential flow of pesticides in unsaturated soil. Journal of Contaminant Hydrology 11, 101–125.

Glass, R.J., Parlange, J.Y., Steenhuis, T.S., 1989. Wetting front instability. 1. Theoretical discussion and dimensional analysis. Water Resources Research 25 (6), 1187–1194.

van Genuchten, M.T., 1980. A closed form equation for predicting the hydraulic conductivity of unsaturated soils. Soil Science Society of America Journal 44, 892–898.

van Genuchten, M.Th., Leij, F.J., Yates, S.R., 1991. The RETC code for quantifying the hydraulic functions of unsaturated soils, Version 1.0. EPA Report 600/2-91/065, US Salinity Laboratory, USDA, ARS, Riverside, CA.

Hansen, E., 1990. Early yields of biomass plantations in the North Central United States. Res. Pap. NC-353. St. Paul, MN, US Department of Agriculture, Forest Service, North Central Forest Experiment Station, 6 pp.

Hansen, E., 1992. Mid-rotation yields of biomass plantations in the North Central United States. Res. Pap. NC-309. St. Paul, MN, US Department of Agriculture, Forest Service, North Central Forest Experiment Station, 8 pp.

Heijs, A.W.J., de Lange, J., Schoute, Th.J.F., Bouma, J., 1995. Computed tomography as a tool for non-destructive analysis of flow patterns in macroporous clay soils. Geoderma 65, 1–19.

Hillel, D., Baker, R.S., 1988. A descriptive theory of fingering during infiltration into layered soils. Soil Science 146, 51–56.

Hoogenboom, G., Jones, J.W., Boote, K.J., 1992. Modeling the growth, development and yield of grain legumes using SOYGRO, PNUTGRO and BEANGRO: a review. Transactions of the ASAE 35 (6), 2043–2056.

Host, G.E., Isebrands, J.G., Theseira, G.W., Kiniry, J.R., Graham, R.L., 1996. Temporal and spatial scaling from individual trees to plantations: a modeling strategy. Biomass and Bioenergy 11, 233–243.

Host, G.E., Theseira, G.W., Heim, C., Isebrands, J.G., Graham, R., 1999. EPIC-ECOPHYS: a linkage of empirical and process models for simulating poplar plantation growth. In: Amaro, A., Tome, M. (Eds.), Empirical and Process Models for Forest Tree and Stand Growth Simulation. Edicos Salamandra, Lisbon, Portugal, pp. 419–429.

Isebrands, J.G., Host, G.E., Lenz, K.E., Wu, G., Stech, H.W., 2000. Hierarchical, parallel computing strategies using component object model for process modelling responses of forest plantations to interacting multiple stresses. In: Cuelemans, R.J.M., Veroustraete, F., Gond, V., Van Rensbergen, J.B.H.F. (Eds.), Forest Ecosystem Modeling, Upscaling, and Remote Sensing. SPB Academic Publishing, The Hague, pp. 123–135.

Jones, C.A., Kiniry, J.R., 1986. CERES-Maize: A Simulation Model of Maize Growth and Development. Texas A&M University Press, College Station, TX.

Li, Y., Ghodrati, M., 1995. Preferential transport of nitrate in soils as affected by earthworm activities. Journal of Environmental Quality 24 (3), 432–438.

Marani, A., Cardon, G.E., Phene, C.J., 1992. CALGOS, a version of GOSSYM adapted for irrigated cotton. I. Drip irrigation, soil water transport and root growth. In: Proceedings, Beltwide Cotton Conference, Nashville, TN, January 6–10, vol. 3, pp. 1352–1357.

Milliken, G., Johnson, D., 1989. In: Analysis of Messy Data, vol. 2. Van Nostrand Reinhold, New York, 199pp.

Oritz, R., 1996. The potential of AMMI analysis for field assessment of Musa genotypes to virus infection. Hortscience 31 (5), 829–832.

Rauscher, H.M., Isebrands, J.G., Host, G.E., Dickson, R.E., Dickmann, D.I., Crow, T.R., Michael, D.A., 1990. ECOPHYS: an ecophysiological growth process model of poplar. Tree Physiology 7, 255–281.

Richardson, C.W., Wright, D.A., 1984. In: WGEN: A Model for Generating Daily Weather Variables. US Department of Agriculture, Agricultural Research Service, Washington, DC, 88 (ARS-8).

Schuster, E.G., Leefers, L.A., Thompson, J.E., 1993. A guide to computer-based analytical tools for implementing national forest plans. USDA-FS General Technical Report INT-296, Intermountain Research Station, Ogden, UT.

Sharpe, P.J.H., 1990. Forest modeling approaches: compromises between generality and precision. In: Dixon, R.K., Meldahl, R.S., Ruark, G.A., Warren, W.G. (Eds.), Process Modeling of Forest Growth Responses to Environmental Stress. Timber Press Inc., Portland, OR, USA, pp. 180–190.

Shinozaki, K., Yoda, K., Hozumi, K., Kira, T., 1964. A quantitative analysis of plant form—the pipe model theory II. Further evidence of the theory and its application in forest ecology. Japanese Journal of Ecology 14 (4), 133–139.

Sinclair, T.R., 1991. Water deficit effects on maize yields modeled under current and "greenhouse" climates. Agronomy Journal 83 (6), 1052–1059.

Theseira, G.W., 1994. Development and testing of an amended GOSSYM model for simulation of asymmetric inputs about the crop row (cotton). PhD dissertation, Mississippi State University, Starkville, MS.

Willers, J.L., Wagner, T.L., Sequeira, R.A., Theseira, G.W., Boykin, D.L., 1995. Analysis of deterministic simulation models using methods applicable to two-way treatment structures without replication. Agronomy Journal 87 (1), 478–492.

Williams, J.R., Dyke, P.T., Jones, C.A., 1983. EPIC: a model for assessing the effects of erosion on soil productivity. In: Laurenroth, W.K. (Ed.), Analysis of Ecological Systems: State-of-the-Art in Ecological Modeling. Elsevier, Amsterdam, pp. 553–572.

Yadav, R., Tyagi, B.S., Horan, J., 1998. AMMI analysis of wheat varietal yield trials. Crop Improvement 25 (1), 105.